Astrochemistry VII – Through the Cosmos
from Galaxies to Planets
Proceedings IAU Symposium No. 332, 2017
M. Cunningham, T. Millar & Y. Aikawa, eds.

doi:10.1017/S1743921317006858

Modeling CO, CO_2 and H_2O Ice Abundances in the Envelopes of Young Stellar Objects in the Magellanic Clouds

Tyler Pauly[1] **and Robin T. Garrod**[2]

[1]Cornell Center for Astrophysics and Planetary Science and Department of Astronomy, Cornell University, Ithaca, NY 14853, USA
email: tap74@cornell.edu

[2]Departments of Chemistry and Astronomy , University of Virginia, Charlottesville, VA 22904-4319, USA

Abstract. Massive young stellar objects (MYSOs) in the Magellanic Clouds (MCs) show infrared absorption features corresponding to significant abundances of CO, CO_2 and H_2O ice along the line of sight, with the relative abundances of these ices varying between sources in the Magellanic Clouds and the Milky Way. We use our gas-grain chemical code MAGICKAL, with multiple grain sizes and grain temperatures, and further expand it with a treatment for increased interstellar radiation field intensity to model the elevated dust temperatures observed in the MCs. We also adjust the elemental abundances used in the chemical models, guided by observations of HII regions in these metal-poor satellite galaxies. With a grid of models, we are able to reproduce the relative ice fractions observed in MC MYSOs, indicating that metal depletion and elevated grain temperature are important drivers of the MYSO envelope ice composition. The observed shortfall in CO in the Small Magellanic Cloud can be explained by a combination of reduced carbon abundance and increased grain temperatures. The models indicate that a large variation in radiation field strength is required to match the range of observed LMC abundances.

Keywords. astrochemistry — ISM: abundances — ISM: molecules — Magellanic Clouds

1. Introduction

Mid-infrared spectral observations of embedded young stellar objects (YSOs) in the Milky Way (MW) and the nearby Magellanic Clouds (MCs) have found a wealth of solid-state features, showing high column densities of ices such as H_2O, CO, CO_2, and CH_3OH. H_2O is the most abundant ice, with a typical column density of $\sim 10^{-4}$ with respect to total hydrogen abundance. In MW YSOs, CO_2 is next most abundant, at an average value of CO_2:$H_2O \simeq 0.2$ Boogert & Ehrenfreund (2004). CO and CH_3OH ices follow at lower abundance, though with nearly an order of magnitude of variation between lines of sight (Gerakines *et al.* 1999; Gibb *et al.* 2004). In contrast, observations of MYSOs in the nearby Magellanic Clouds show a marked difference in ice abundances. Shimonishi *et al.* (2010) and Oliveira *et al.* (2011) detected H_2O, CO and CO_2 ice in MYSOs in the Large Magellanic Cloud (LMC); they found that LMC sources had elevated CO_2 ice or depleted H_2O ice when compared to galactic counterparts, with an average value for CO_2:H_2O of 0.32. Oliveira *et al.* (2011, 2013) found only an upper limit for CO ice in all Small Magellanic Cloud (SMC) sources studied, with abundances (with respect to their H_2O columns) a factor of three to ten lower than their galactic counterparts. Oliveira *et al.* (2011) and Shimonishi *et al.* (2016) provided additional near-infrared spectra of

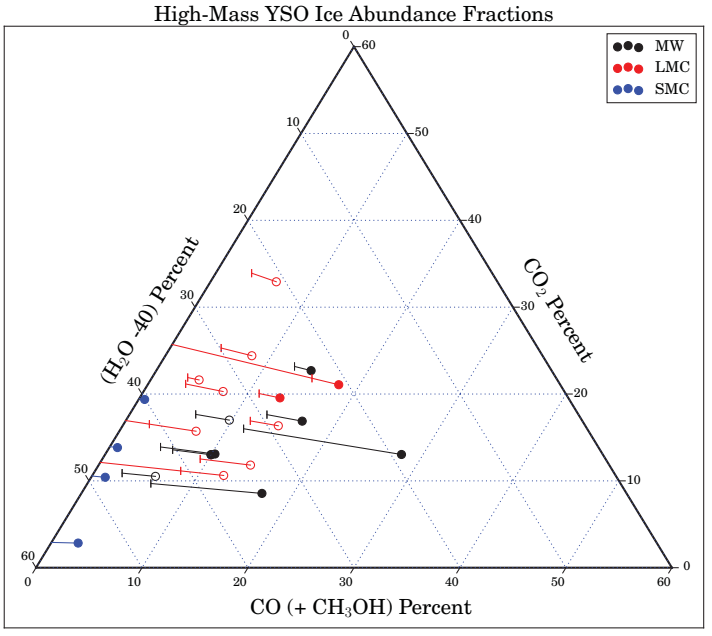

Figure 1. The relative abundances of the four major ices in massive young stellar objects in the Milky Way (black), LMC (red), and SMC (blue). SMC sources have only upper limits on CO and no information on CH_3OH; SMC points show the composition at the upper limit value with a line drawn to zero CO abundance. For LMC and Milky Way sources, the vertical tick shows the H_2O:CO:CO_2 composition, while the circles show the composition including CH_3OH ice as H_2O:(CO+CH_3OH):CO_2. For LMC sources with only an upper limit on CO, lines have been drawn to zero CO abundance, while sources with an upper limit on CH_3OH ice have an open circle. (Ternary figure style from Harper *et al.* 2015)

a sample of LMC MYSOs, with detections or upper limits for CH_3OH ice towards all sources studied.

These ices are found in the dense, cold envelopes surrounding the highly luminous central source, and they hold information on their past collapse history via e.g. the polar to apolar ratio of the CO and CO_2 ice features (Gibb *et al.* 2000). They are processed to some extent by the internal radiation source, though the source-to-source variation of this processing is expected to be large. Local environment also plays a role, with changes in the nearby interstellar radiation field (ISRF) or the cosmic ray ionization rate affecting gas and grain surface chemistry. Additionally, variations in the underlying elemental abundances of the collapsing cloud will influence the general chemistry and ice column densities.

We collate observations of MYSOs for which H_2O, CO, CO_2 and CH_3OH detections or upper limits are available, excluding CH_3OH for SMC sources (toward which no measurements of CH_3OH have yet been achieved). Figure 1 shows the total observation sample we will use for model comparison, plotted in a ternary H_2O:CO_2:CO ice diagram. The ternary plot describes the relative abundances of this three-component ice system; importantly, we also consider methanol (CH_3OH) ice, a key component for galactic YSOs and now detected toward some LMC MYSOs. To include this fourth component on a ternary diagram, we include a second point for those sources with methanol detections or upper limits; these points show the fractional abundance of H_2O:CO_2:(CO+CH_3OH). This pairing choice of (CO+CH_3OH) is chemically motivated, as CH_3OH is primarily formed from the successive hydrogenation of CO on grain surfaces (Watanabe & Kouchi

https://doi.org/10.1017/S1743921317006858 Published online by Cambridge University Press

2002; Cuppen *et al.* 2009). The figure shows a transition in composition between environments, with some blending between some LMC and galactic sources.

Using the single-point free-fall collapse model detailed by Garrod & Pauly (2011) and Pauly & Garrod (2016), we investigate parameters responsible for the chemical variation amongst MYSOs in the galaxy, LMC and SMC. We take the elemental abundances and dust temperatures of the forming YSO to be the parameters of interest for this model study.

2. Model Methods

We use the gas-grain chemical code MAGICKAL and its associated chemical network, first presented by Garrod (2013) and updated by Pauly & Garrod (2016) to include a grain-size distribution consisting of five grains. The model features 475 gas-phase species and 200 grain surface species with a network of roughly 9000 reactions and processes. Grain surface species are tracked in two separate phases, surface and mantle; the surface species participate in desorption, reaction and diffusion across grain sites, while the ice mantle is treated as a separate phase that is coupled to the surface. Bulk diffusion in the mantle ice is treated explicitly, allowing reactions within the mantle, as well as exchange between surface and mantle components; however, for the low temperatures involved in this work we treat the mantle phase as inert except for the transfer of surface material into the bulk, as the mantle grows. The model uses the modified-rate approach detailed in Garrod (2008) (method "C") to account for possible stochastic effects in the surface chemistry. The chemical network also includes photodissociation and photoionization processes, with photons sourced either from the ambient field or the cosmic ray-induced UV field.

We model the evolution of dust temperature as a function of the visual extinction and dust radius, following methods outlined in Garrod & Pauly (2011). We add an additional variable in a model-dependent interstellar radiation field (ISRF). We approximate the ISRF in various environments by modifying the multi-component fit from Zucconi, Walmsley, & Galli (2001) for the Milky Way. The fit includes contributions from three discrete stellar black-body populations, both hot and cool diffuse dust components, and the cosmic microwave background. To simulate variation in ISRF intensity in the Magellanic Clouds, we scale the stellar components uniformly, from the base factor of 1.0 to 3.0 in increments of 0.5. The resulting dust temperatures shift by 3-5 K at $A_V \sim 1$ and 1.5 K at $A_V \sim 10$, with the smallest grains having the highest temperature. The increase in A_V during the collapse process results in a general cooling and a flattening of the temperature distribution with respect to grain size; the temperature difference between the smallest and largest grains shrinks from 5 K to <1 K.

To model the ISM of the metal-poor galaxies, we deplete the heavy elemental abundances in the initial setup of our models. The Magellanic Clouds have bulk metallicity of $Z_{LMC} \sim 0.4Z_\odot$ and $Z_{SMC} \sim 0.2Z_\odot$ (Russell & Dopita 1992). Kurt & Dufour (1998) collated observations of six SMC HII regions to find the mean abundances of carbon, nitrogen and oxygen. Peimbert (2003) collected a UV-visible spectrum of 30 Doradus in the LMC; with 269 identified emission lines, they calculate the total abundance of carbon, nitrogen and oxygen. These two studies provide us with ISM compositions to model the metal-depleted environments associated with star formation in the Magellanic Clouds. The abundance values are shown in Table 1; these abundances will be referred to as MW, LMC, and SMC.

https://doi.org/10.1017/S1743921317006858 Published online by Cambridge University Press

Element	MW	LMC	SMC
H	5.000(-5)	5.000(-5)	5.000(-5)
H_2	0.499975	0.499975	0.499975
O	3.200(-4)	2.140(-4)	1.047(-4)
C^+	1.400(-4)	6.310(-5)	1.585(-5)
N	7.500(-5)	1.12(-5)	2.820(-6)
C/O Ratio	0.438	0.295	0.151

Table 1. Elemental abundances, listed with respect to total hydrogen number density, n_H. The first column represents galactic abundances, taken from Garrod & Pauly (2011). The second column is used as representative values for the LMC, taken from Peimbert (2003). The final column is the most depleted abundances considered and are taken from the sample of SMC HII regions in Kurt & Dufour (1998).

3. Results & Discussion

We computed a grid of fifteen models by multiplying the stellar component of the ISRF with values of [1.0, 1.5, 2.0, 2.5, 3.0] and varying the elemental abundances between initial elemental abundance setups MW, LMC, and SMC. H_2O is the dominant ice component in nearly all models as expected, following observations. The collapse is complete by $\sim 8 \times 10^5$ ($10^{5.9}$) years; for models with 1.0, 1.5 or 2.0 stellar intensity, this causes dust temperatures to drop below an efficiency threshold for producing CO_2 from CO + OH, identified by Garrod & Pauly (2011). CO mobility on the grain surface is sufficiently slowed at temperatures below $\sim$ 12 K; by this point, the fractional abundance of CO grows above that of CO_2. Models with 2.5 or 3.0 stellar intensity never drop below this temperature threshold, and as a result high CO_2 ice abundances are found throughout those models.

CH_3OH ice is formed via the hydrogenation of surface CO, which is only present after temperatures drop below the 12 K threshold. For MW models with abundant CO ice, the efficiency of CH_3OH formation appears low, with the abundance ratio of CH_3OH:CO ranging from 1:2 to 1:5. However, in SMC models with low CO surface abundance, surface CH_3OH can be equal in abundance to CO, and these molecules are similarly abundant throughout those model runs.

The hydrides CH_4 and NH_3 appear to track closely the elemental abundance of their atomic parent, with some dependence on temperature shown for models with galactic elemental abundances.

Figure 3 shows the model results overlaid on the observations. For each model we plot two points per panel; for the left panel, the smaller leftward point shows the ice composition at $8{\times}10^5$ years, while the large rightward point shows the composition at 10^6 years. The right panel shows the same models at times of 10^6 years and $5{\times}10^6$ years. The choice of time spent at post-collapse density is arbitrary, and because physical conditions do not change significantly during this time, the composition follows a roughly straight line between these points. The MW and SMC abundance models appear to match observations more closely at earlier times, while the LMC observations have variation such that model matches are found at both early and late times.

Models with MW abundances show compositions enriched in CO_2 and [CO+CH_3OH], with the relative enrichment between the two set by the stellar flux parameter. As no observations lie near the high stellar flux galactic abundance models, these models do not appear to represent any observed MYSO and can be ignored.

LMC MYSOs demonstrate large variation in composition, from extreme [CO+CH_3OH] depletion (as in SMC sources) to highly enriched in CO_2. Models with LMC-like elemental abundances fall across the ensemble of LMC MYSOs, though there is considerable overlap

https://doi.org/10.1017/S1743921317006858 Published online by Cambridge University Press

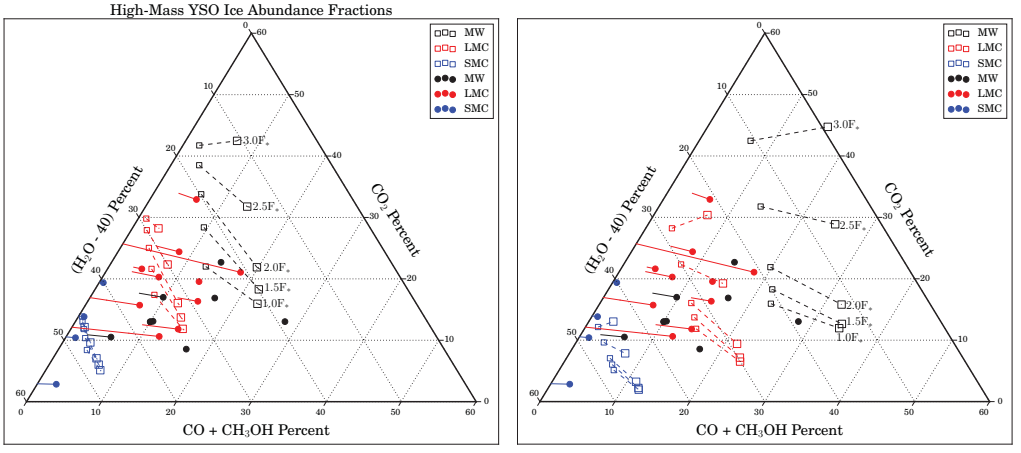

Figure 2. These panels overlay the model results on the observations from Figure 1. With matching colors for model elemental abundances to source environment (MW, LMC, SMC), models with increasing stellar flux parameter move upwards on the plot, with galactic chemical abundance models labeled. For each model, two points are plotted; for the top panel, the smaller leftward square shows the ice composition at the time of collapse completion ($\sim 8\times10^5$ years), while the larger rightward square shows the composition at 10^6 years. For the lower panel, the leftward square shows the composition at 10^6 years, while the rightward square shows the values for 5×10^6 years. (Ternary figure style from Harper *et al.* 2015)

between LMC and galactic sources. The models separate cleanly on this plot, implying additional effects not addressed in the model setup. Variation in local metallicity may cause blending, as metal-poor MW YSOs may appear chemically similar to LMC MYSOs. Parameters beyond our model, such as variation in collapse speed or ice processing may also play a role. Models are able to fit LMC observations at the full range of stellar flux parameter tested.

Models with the most depleted elemental abundances fall near the observed SMC MYSOs, matching the low (undetected) CO abundance and presence of CO_2. The models lying closest to observed YSO abundances have high stellar flux values, though the models cannot fully reproduce the spread in CO_2 abundances and typically overproduce [CO+CH_3OH]. Of note, the composition of SMC models shows a roughly equal abundance of surface CO and CH_3OH, while observational upper limits exist only for CO. Tightening the abundance constraints on these two species would provide strong evidence for the validity of our [CO+CH_3OH] surface chemistry.

The increased CH_3OH abundance relative to CO in SMC models is an unexpected result. CH_3OH formation requires CO surface residence times to be longer than the mantle deposition time scale, to allow sufficient time for hydrogenation. In this way, the balance between CO and CH_3OH is determined primarily by the accretion rate of elements heavier than hydrogen. With long CO surface residence times, CO_2 production will also be increased if dust temperatures are above the necessary threshold for CO surface mobility.

The models produce a reasonable fit to observations, though a general trend exists in overproduction of [CO+CH_3OH]. This may not be a simple model issue but instead a comparison of model results to observations in different physical regimes. These MYSOs are highly luminous objects, and thermal processing of the envelope is likely to have occurred in many sources. In this case, the most volatile ices may be under-abundant

https://doi.org/10.1017/S1743921317006858 Published online by Cambridge University Press

due to evaporation when compared to the final model output, which ends prior to a grain heating and ice evaporation phase.

4. Summary

Our results suggest that gas-grain models of cold cloud collapse can produce ice mantle abundances that match reasonably well to observations in a variety of environments. We conclude that:

- The values of ISRF intensity and elemental abundances chosen provide an adequate distribution of ice abundances that cover the observed ice abundances in YSOs. Models with strongly enhanced ISRF intensity at MW elemental abundances are excluded, while SMC models with enhanced ISRF are preferred.
- LMC models lie near observed YSOs for every value of the ISRF intensity modeled, characterizing the large spread in LMC YSO ice abundances. This may be indicative of large local fluctuations in the LMC ISRF.
- The ISRF intensity strongly affects the relative abundance of CO_2 to CO/CH_3OH, with higher ISRF values leading to CO_2 enhancement. This is caused by a temperature threshold for CO mobility on grain surfaces, leading to efficient production of CO_2 at dust temperatures $\gtrsim 12$ K.
- Increasing model elemental abundances (and corresponding C/O ratio) decreases the H_2O abundance against the other ices; this is evidenced by model values moving parallel to the H_2O ternary axis with changes in elemental abundance.
- Our models indicate that the lack of CO in SMC sources is most likely caused by a combination of low elemental abundances and high ISRF intensity.
- CH_3OH abundance is found to be enhanced in low-metallicity environments. This will be important for complex organic molecule production in LMC and SMC hot core models.

We leave some issues to be addressed in future work. Thermal processing of the ice is important for matching observed ice abundances, and it is not included in these models. We find significant growth in the [dust+mantle] radius, which affects both the dust temperature and surface chemistry; however, we assume a Q_{abs} of carbonaceous dust for temperature calculations, though the Q_{abs} of ice will differ. We also use a grain size distribution found for silicate grains; this could be resolved by using values for silicate or carbonaceous grains throughout, or by attempting to model both populations.

Future models could investigate the dependence on cosmic ray ionization rate, a parameter with large variation across the LMC. The rate of collapse may also be important, as it sets the heavy atom accretion rate. Follow-up models will address behavior in collapse to higher densities ($\sim 10^7$ cm^{-3}), including a warm-up phase for comparison to a newly detected hot core in the LMC (Shimonishi *et al.* 2016).

References

Boogert, A. C. A. & Ehrenfreund, P. 2004, *ASPC*, 309, 547
Cuppen, H. M., van Dishoeck, E. F., Herbst, E., & Tielens, A. G. G. M. 2009, *A&A*, 508, 275
Garrod, R. T. 2008, *A&A*, 491, 239
Garrod, R. T. & Pauly, T. 2011, *ApJ*, 735, 15
Garrod, R. T. 2013, *ApJ*, 765, 60
Gerakines, P. A., Whittet, D. C. B., Ehrenfreund, P., Boogert, A. C. A., Tielens, A. G. G. M., Schutte, W. A., Chiar, J. E., van Dishoeck, E. F., Prusti, T., Helmich, F. P., & de Graauw, T. 1999, *ApJ*, 522, 357

https://doi.org/10.1017/S1743921317006858 Published online by Cambridge University Press

Gibb, E. L., Whittet, D. C. B., Schutte, W. A., Boogert, A. C. A., Chiar, J. E., Ehrenfreund, P., Gerakines, P. A., Keane, J. V., Tielens, A. G. G. M., van Dishoeck, E. F., & Kerkhof, O. 2000, *ApJ*, 536, 347

Gibb, E. L., Whittet, D. C. B., Boogert, A. C. A., & Tielens, A. G. G. M. 2004, *ApJS*, 151, 35

Harper, M., Weinstein, B., Simon, C., chebee7 i, Swanson-Hysell, N., The Gitter Badger, Greco, M., & Zuidhof, G. 2015, *doi* = 10.5281/zenodo.34938

Kurt, C. M. & Dufour, R. J. 1998, *RMxAC*, 7, 202

Oliveira, J. M., van Loon, J. T., Sloan, G. C., Indebetouw, R., Kemper, F., Tielens, A. G. G. M., Simon, J. D., Woods, P. M., & Meixner, M. 2011, *MNRAS*, 411, 36

Oliveira, J. M., van Loon, J. T., Sloan, G. C., Sewiło, M., Kraemer, K. E., Wood, P. R., Indebetouw, R., Filipović, M. D., Crawford, E. J., Wong, G. F., Hora, J. L., Meixner, M., Robitaille, T. P., Shiao, B., & Simon, J. D. 2013, *MNRAS*, 428, 3001

Pauly, T. & Garrod, R. T. 2016, *ApJ* 817, 146

Peimbert, A. 2003, *ApJ* 584, 735

Russell, S. C. & Dopita, M. A. 1992, *ApJ* 384, 508

Shimonishi, T., Onaka, T., Kato, D., Sakon, I., Ita, Y., Kawamura, A., & Kaneda, H. 2010, *A&A*, 514, 12

Shimonishi, T., Dartois, E., Onaka, T., & Boulanger, F. 2016, *A&A* 585 107

Shimonishi, T., Onaka, T., Kawamura, A., & Aikawa, Y. 2016, *ApJ* 827, 72

Watanabe, N. & Kouchi, A. 2002, *ApJL* 571, 173

Zucconi, A., Walmsley, C. M., & Galli, D. 2001, *A&A* 376, 650